Electronic supplementary information (ESI)

Gold-loaded nanoporous superparamagnetic nanocubes for catalytic signal amplification in detecting miRNA

Mostafa Kamal Masud[a,b], Md. Nazmul Islam[b,c], Md. Hakimul Haque[c,d], Shunsuke Tanaka,[a] Vinod Gopalan[d], Gursel Alici,[e] Nam-Trung Nguyen[b], Alfred King-yin Lam[d], Md. Shahriar A. Hossain[a*], Yusuke Yamauchi[a*], and Muhammad J. A. Shiddiky[b,c*]

Table of contents:

1. Experimental

1.1 Materials

Unless otherwise stated, the reagents and chemicals used for the conducting experiments were of analytical grade. Polyvinylpyrrrolidone (PVP) and potassium hexacyanoferrate (III) were purchased from Nacalai Tesque and Merck KGaA, Germany respectively. Reagent grade hexaammineruthenium(III) chloride (RuHex), phosphate buffer saline (PBS) tablet (0.01M phosphate buffer, 0.0027M potassium chloride and 0.137M sodium chloride, pH 7.4 at 25ºC) were purchased from Sigma-Aldrich (Australia). Analytical grade hydrochloric acid (HCl) was purchased from Chem-supply (Australia). Tris was obtained from VWR Life science (Australia), glassy carbon electrode (GCE) was purchased from CH instrument (USA). Screen-printed carbon electrode (SPCE) with a three-electrode system printed on a ceramic substrate (length 34 × width 10 × height 5 mm) (DRP-150) from Dropsens (Spain). In the three-electrode system, working (4 mm diameter), counter and reference electrodes were carbon, platinum and silver-modified. All chemicals and reagents were used as received without additional purification. UltrapureTM DNase/RNase-free distilled water (Invitrogen, Australia) was used throughout the experiments. Oligonucleotides were acquired from Integrated Technologies, USA and sequences are shown in table S1.

Table S1. Oligonucleotide sequences

Oligos	5′-Sequences-3′
Biotinylated miR-21 capture probe	TGA CCG ACC CAG TGA GGA AGT TTT CTC T/ 3Bio
Synthetic miR-21 sequence	AGA GAA AAC UUC ACU GGG UCG GUC A

1.2 Instrumentations

Scanning electron microscope (SEM) images were taken with a Hitachi S-4800 scanning microscope with the accelerating voltage of 10 kV. Wide-angle powder X-ray diffraction (XRD) patterns were obtained with a Rigaku RINT 2500X diffractometer using monochromated Cu Kα radiation (40 kV, 40 mA) at a scanning rate of 0.5 ° min^{-1}. The

elemental chemical analysis of the nanocubes was performed by X-ray photoelectron spectroscopy (XPS, PHI Quantera SXM, ULVAC-PHI Inc., Japan). All samples were degassed in vacuum before carrying out the measurements. All electrochemical measurements were performed with a CHI650 electrochemical workstation. (CH Instrument, USA). Cyclic voltammetry (CV) and chronoamperometry experiments were done in a single-compartment cell with a 3-mL volume. A conventional three-electrode system, comprising a bare or modified GCE, a platinum auxiliary electrode, and an $Ag/AgCl_3$ 1.0 M NaCl reference electrode (CH Instrument, Inc. USA), was used for the measurement of electrocatalytic activity. Chronocoulometry (CC) measurements were carried out using 80µL volume on SPCE between 0 and -500mV, 25 ms pulse width and 2 ms sample interval. A temperature and time control ultrasonic water bath (Soniclean, Australia) was applied for dispersion of $Au@NPFe_2O_3NC$ nano-hybrid before applying to the electrode surface.

1.3 Synthesis and characterisation of $Au@Fe_2O_3NC$

Porous iron oxide nanocubes ($NPFe_2O_3NC$) were prepared from Prussian blue (PB) nanocubes (NC) *via* calcination of PB at 250 °C following our previous report.[1-2] Concisely, 6.0 g of PVP (polyvinylpyrrolidone) (K30) and 264 mg of $K_3[Fe(CN)_6].3H_2O$ were dissolved in 80mL 0.01M HCl solution followed by the magnetic stirring for 30 min to produce a clear yellow solution. The obtained solution was then heated at 80 °C for 30 h in an electronic furnace, and the produced precipitates were collected by centrifugation. PB NCs of 80 nm sized were obtained after 24 hr hours drying at room temperature. The obtained PB NCs are in cubic shape which is a typical PB material (**Fig. S1A**). The prepared PB NCs show the same face-centered cubic diffraction patterns that of the bulk PB crystals (JCPDS card 73-0687) (**Fig. S1C**). The prepared PB NCs was highly pure as there were no peaks derived from impurities in XRD pattern. In the parent PB crystals, iron atoms are separated by cyano-bridges, which facilitates the favourable conditions for Fe_2O_3 particles during the calcination process. To prepare nanoporous iron oxide, 50 mg of obtained PB powders was taken in a melting pot and heated in an electronic furnace to achieve complete thermal decomposition. The powders were then allowed to cool inside the furnace. The morphology of the prepared PB-derived iron oxide remains as NCs, but their sizes were slightly reduced and surface roughness was increased (**Fig. S1B**).

For loading AuNPs on to the porous nanocube, 250 mg of iron oxide nanocubes were dispersed in sodium citrate solution followed by the addition of 3 mL of 10 mM $HAuCl_4$

solution. The mixed solution was then incubated under ice-water bath till its temperature was stable. Then, sodium borohydride solution as a reducing agent was quickly added into the above solution under vigorous stirring. After reacting for 10 min, the product was washed and collected by successive centrifugation. After deposition of Au NPs, uniformly sized Au NPs are distributed on the surface of nanoporous iron oxide NCs (**Fig. 1A**). The loading amount of Au nanoparticles is around 2 wt% in the product (Au@NPFe$_2$O$_3$NC) (**Fig. 1B**). The XRD pattern shows the diffraction peaks derived from Au, α-Fe$_2$O$_3$, and γ-Fe$_2$O$_3$ (**Fig. S1D**). This sample is found to be superparamagnetic from the complete reversibility of the *M-H* curve recorded at room temperature (300 K). The S-shaped hysteresis loops are shown in **Fig. S2** with the negligible coercive field (H_c) are a typical characteristic of superparamagnetic nanoparticles.[3-5] The saturation magnetisation (M_s) reported in this study is 16 emu g^{-1} at 300 K for Au@NPFe$_2$O$_3$NC. Due to this sufficient M_s value, the samples can be easily collected by a neodymium magnet. With the loading amount of Au nanoparticles, the M_s value is decreased because of the non-magnetic property of Au.

1.4 Electrochemical measurement of catalytic activity

A GCE was polished using 0.3 and 0.05 mm alumina slurry (CH Instrument, Inc. USA) followed by rinsing with an adequate amount of water. After successive sonication with nitric acid and water, the electrode was again rinsed thoroughly using DI water, allowed it to dry at room temperature. A mirror surface was formed. To assess the electrocatalytic activity of Au@NPFe$_2$O$_3$NC, 5μg of a colloidal suspension of Au@NPFe$_2$O$_3$NC were drop-dried onto the surface of the clean GCE electrode. The electrocatalytic activity Au@NPFe$_2$O$_3$NC towards the reduction of RuHex was studied using cyclic voltametric technique at room temperature with the conventional three-electrode system using Au@NPFe$_2$O$_3$NC-modified GCE as the working electrode.

The chronoamperometric experiment was also carried at -0.25V versus Ag/AgCl at optimum condition. The current response due to the successive addition of RuHex (10 – 1100 μM) was monitored. The apparent Michaelis-Menten constant (K_m^{app}) of GCE/Au@NPFe$_2$O$_3$NC can be determined from the Michaelis-Menten equation;[6]

$$I = \frac{I_{max}[S]}{K_m^{app} + [S]} \ldots \quad \ldots \quad \ldots (1)$$

In this equation, I is the steady state current, I_{max} is the maximum current measured under the condition of enzyme saturation, [S] is the substrate concentration, and K_m^{app} is the Michaelis-Menten constant, which is equivalent to the substrate concentration at the conversion rate is half of I_{max}. K_m^{app} is the indicator of enzyme or catalyst affinity to substrates. A high K_m^{app} indicates week affinity while a low value suggests a high affinity. The rearrangement of Michaelis-Menten equation gives the electrochemical version of Lineweaver–Burk equation,[7] which also widely used to determine electrocatalytic enzyme kinetics terms K_m^{app} and I_{max}.

$$\frac{1}{I} = \frac{K_m^{app}}{I_{max}} \frac{1}{[S]} + \frac{1}{I_{max}} \ldots \quad \ldots \quad \ldots (2)$$

1.5 Determination of the surface area of the electrodes

The effective surface areas of both GCE and SPCE were determined by the measurement of the peak current obtained as a function of scan rate under cyclic voltammetric conditions for the one-electron reduction of $[Fe(CN)_6]^{3-}$ [2.0 mM in PBS (0.5 M KCl)] and by using the Randles-Sevcik equation (eq 3),[8,9]

$$i_p = (2.69 \times 10^5)\ n^{3/2} A D^{1/2} C v^{1/2} \ldots \quad \ldots \quad (3)$$

where, i_p is the peak current *(*A), n is the number of electrons transferred ($Fe^{3+} \rightarrow Fe^{2+}$, $n = 1$), A is the effective area of the electrode (cm^2), D is the diffusion coefficient of $[Fe(CN)6]^{3-}$ (taken to be $7.60 \times 10^{-5} cm^2 s^{-1}$), C is the concentration (mol cm^{-3}), v is the scan rate (Vs^{-1}).

1.6 Preparation of the miRNA recognition interface

Before the adsorption of miRNA, SPCE was washed and cleaned by rinsing with excess amount of miliQ water. To attach Au@NPFe_2O_3NC to SPCE surface, the electrode was positioned on a permanent magnet so that the surface is centred to the magnet and 5µg of Au@NPFe_2O_3NC was employed onto the electrode surface (see Fig. 3). The Au@NPFe_2O_3NC was allowed to attach onto the surface for 45 min. The electrode was then washed with 10 mM PBS to remove unattached or loosely attached particles from the electrode surface.

1.7 RNA Extraction from cell lines and tissue samples

Two oesophageal squamous cell carcinoma cell lines (HKESC-1 and HKESC-4) were used for this study. These cells were cultured in minimum essential medium alpha (MEMα growth medium, Gibco (ThermFisher scientific, Waltham, MA, USA) medium with non-essential amino acids and supplemented with 10% fetal bovine serum (FBS, Gibco), 100 µg/mL penicillin (Gibco) and 100 units/mL streptomycin (Gibco) in a humidified cell culture incubator containing 5% CO_2 at 37 °C. Four matched fresh oesophageal squamous cell carcinoma (ESCC) and non-neoplastic tissues were snap-frozen and sectioned into 10µm slices using a cryostat (Leica CM 1850 UV, Wetzlar, Germany). Tissue sections were stained with haematoxylin and eosin for RNA extraction. Ethical approval was obtained from the Griffith University Human research ethics committee for the use of ESCC tissues (GU Ref Nos: MED/19/08/HREC).

Total RNA was isolated and purified from all tissue samples following the manufacturer's recommendations of all prep DNA/RNA mini kit (Qiagen, Hilden, NRW, Germany). Briefly, tissue samples were suspended in 0.01M PBS following a digestion step to remove the debris, protein and DNA in the solution *via* proteinase and DNase enzymes, respectively. The digested proteins and DNA were then removed by the centrifugation of the solution in a spin column. The purified RNA was eluted from the column using 100 µL of elution buffer. To evaluate the quality and quantity of RNA, agarose gel (1.5%) electrophoresis and Nanodrop spectrophotometric analysis (BioLab, Ipswich, MA, USA) using 260:280 ratio was performed. The concentration of RNA was noted in ng/µl and stored at -80^{O}C until assayed.

1.8 Isolation of target miRNA

Target miRNA was captured by hybridizing with magnetic beads functionalized complementary capture probe followed by magnetic isolation and heat release of miRNA in accordance with our previous method.[10] Briefly, 10µL of commercial streptavidin-labelled magnetic beads (Dynabeads® MyOne™ Streptavidin C1, Invitrogen, Australia) was washed with binding and washing (B and W) solution followed by 20 min incubation with an equal volume of 10µM biotinylated capture probes. The functionalized beads were washed and re-suspended in the 10µL 5x SSC (saline sodium citrate) buffer. 10µL of target miRNA (pre-

adjusted 50ng total RNA from tissue samples to 10µL with RNase-free water or various concentration of synthetic miRNA) was then mixed with beads functionalized capture probe. After 20 min of incubation and washing with the (B and W) solution, the miRNA attached beads were isolated with an external magnet and resuspended in 9 µL of RNase free water. The resuspended miRNA mixture was heated for 2 min at 95ºC, immediately attached the beads with magnet and supernatant containing the desired miRNA was collected. Before applying miRNA on to Au@NPFe_2O_3NC-modified electrode, the miRNA was diluted two times with 5XSSC buffer.

1.9 Electrochemical detection of adsorbed microRNA

For detecting miRNA, 5µg of Au@NPFe_2O_3NC was added on the SPCE. The electrode was then positioned on a permanent magnet (see Fig. 3). 4 µL of target miRNA sample were then incubated onto the magnetically attached Au@NPFe_2O_3NC/SPCE surface for 30 minutes followed by PBS washing. The electrode was then incubated with 7µL of 50µM Ruhex so that positively charged Ru^{3+} can bound with the negatively charged phosphate backbone of adsorbed miRNA. The electrode was then washed with PBS before performing CC measurement. CC measurement was then carried out in 10mM Tris buffer (pH 7.4, 80µL) with a potential step of 5 mV and pulse width of 250 ms, and a sample interval of 2 msec. Using CC, the amount of miRNA adsorbed onto the Au@NPFe_2O_3NC/SPCE surface was then calculated from the number of cationic redox molecules (RuHex) electrostatically associated with the surface-attached anionic phosphate backbone of miRNA. The total charge Q at a time *t* can be expressed by the integrated Cottrell equation;[11,12]

$$Q = \frac{2nFA_0^{1/2}C_0^*}{\pi^{1/2}}t^{1/2} + Q_{dl} + nFA\Gamma_0 \ldots \qquad \ldots \qquad \ldots (4)$$

where, *n* is number of electrons involved in electrode reaction, *F* is Faraday constant (C/equivalent), *A* is the electrode area (cm^2), D_o is the diffusion coefficient (cm^2/s), C_o* *is the* bulk concentration (mol/cm^2), Γ_0 is represent the amount of RuHex-confined near electrode surface and $nFA\Gamma_0$ (kwon as surface excess) is the charge obtained by adsorbed miRNA. CC curves were constructed by plotting the charge flowing through the RNA-attached electrode versus square-root of time ($t^{1/2}/s^{1/2}$) in the presence and absence RuHex. *Q* and Q_{dl} were estimated from the intercept of these two curves at $t = 0$. Therefore, *Q* represents the total

charge comprising both Faradic and non-Faradic (capacitive) charges. Hence, the corresponding charge of RuHex (electrostatically bound to surface confined RNA) can be calculated as,

$$Q_{RNA} = Q - Q_{dl} \ldots \quad \ldots \quad \ldots (5)$$

And the saturated surface density of RuHex could be used to calculate surface attached miRNA using the following equation;

$$\Gamma_{RNA} = \left(Q_{RNA} N_A / nFA\right)\left(z/m\right) \ldots \quad \ldots \quad \ldots (6)$$

where, n is the number of electrons involved in the reaction (n = 1), A is the working electrode area, N_A is the Avogadro's number, m is the number of nucleotides in the RNA, and z is the charge of redox molecules (for RuHex, z = 3).

For Fig 4B, using the equation (5) and (6), the surface density of miR-21 on the electrode surface were calculated to be 8.52×10^{13} and 1.6×10^{13} moleculescm^{-2} for 1.0 μM and 100 fM of miRNA respectively.

1.10 Quantitative reverse-transcription polymerase chain reaction (RT-qPCR)

cDNA conversion was first carried out using miScript Reverse Transcription kit (Qiagen, Germany) as previously described.[13,14] Each cDNA sample of 30 ng/μL was allocated and stored at -20ºC for RT-qPCR analysis. The level miR-21 expression was amplified using the primers: forward, 5′- CGGCGGTAGCTTATCAGACTGA-3′ and reverse, 5′-GTGCAGGGTCCGAGGT-3′. Primer pairs were purchased from Integrated DNA Technologies (USA). RT-qPCR was achieved in a total volume of 10 μL reaction mixture comprising 5 μL of 2xSensiMix SYBR No-ROX master mix (Bioline, UK), 1 μL of each 1 μmole/μL primer, 1 μL of cDNA at 30 ng/μL and 2 μL of Nuclease-free water. Thermal cycling was initiated with a first denaturation step at 95°C for 10 minutes followed by 40 cycles of 95°C for 15 seconds (denaturation), 60°C for 30 seconds (annealing), and 72°C for 30 seconds (extension). Expression levels were normalized against the endogenous U6 control gene, which was amplified in the same run and following the same procedure described above. The sequences of the U6 primers were as follows: forward, 5'-

GCTTCGGCAGCACATATACTAAAAT-3' and reverse, 5'- GTGCAGGGTCCGAGGT-3'. Assays were accomplished in triplicate to verify the results and a non-template control was included in all the experiment. Data analysis of miR-21 expression was performed as previously reported.[13]

2. Supplementary Table

Table S1: Comparative Analytical performance of electrochemical sensors for microRNA

Assay	Target	LOD	Comparison of LOD (approx.)	Remarks	Ref.
Photo-electrochemical biosensing platform based on DNA–CdS quantum dots (QDs) sensitized single-walled carbon nanotubes (SWCNTs)-COOH	miR-7f	34 fM	~3 times lower (100 fM *versus* 34 fM)	This method uses cumbersome ssDNA-Cds QDs labelling and adopted DNase I amplifications.	15
Electrical silicon nanowires (SiNW) biosensor based on peptide nucleic acid (PNA)	let-7b and let-7c	1fM	10 times 1ower (100 fM *versus* 1 fM)	Detection is based on tedious, time consuming PNA functionalization of SiNW followed by hybridization with target miRNA. Moreover, the sensor is not reusable as chemical treatment and heat denaturation (~95 ◦C) may damage SiNW properties.	16
Electrochemical detection based on Poly(A) Extensions	miR-107	10 fM	~3 times lower (100 fM *versus* 10 fM)	This techniques utilizes E. Coli Poly(A) extension reaction, required extra incubation time and heating, which may cause target miRNA degradation.	10
Chronocoulometric detection based on rolling circle Amplification (RCA)	miR-143	100 fM	Similar (100 fM *versus* 100 fM)	This platform uses complicated RCA amplification and usually it is not capable of amplifying a satisfactory length of nucleic acids.	12
Differential pulse voltammetry using an redox complex of osmium (VI) and 2,2′-bipyridine	miR-261 and miR-522	2 nM	~1 x10^4 times higher (100 fM *versus* 10 nM)	In this methods, labelling of miRNA with Os(VI)bipy may increase the risk of contamination or sample degradation.	17
Amperometry using Pd nanoparticles as enhancer and linker	miR-155	1.87 pM	~60 times higher (100 fM *versus* 1.87 pM)	This method involves multi-steps electrode surface modifications and based on tedious Thi as alinker.	18

Chronoamperometry based on magnetic bead based capture	miR-222	7.0 pM	~20 times higher (100 fM *versus* 7.0 pM)	It relies on enzymatic treatment, required biotinylation of target RNA, and quantification of miRNA is carried out via p-aminophenol followed by enzyme kinetics (indirect way).	19
Chronocoulometric detection based on electrocatalytic nanoporous superparamagnetic nanocubes.	miR-21	100 fM	This work	Unlike to the traditional affinity-based detection, this assay exploits magnetic nanoparticle-based intimate mixing, separation and purification of miRNA which reduce the matrix effects of the biological samples. It avoids conventional hybridization chemistries and need of expensive electrochemical tags or labelling or enzymatic amplifications.	This work

3. Supplementary Figures

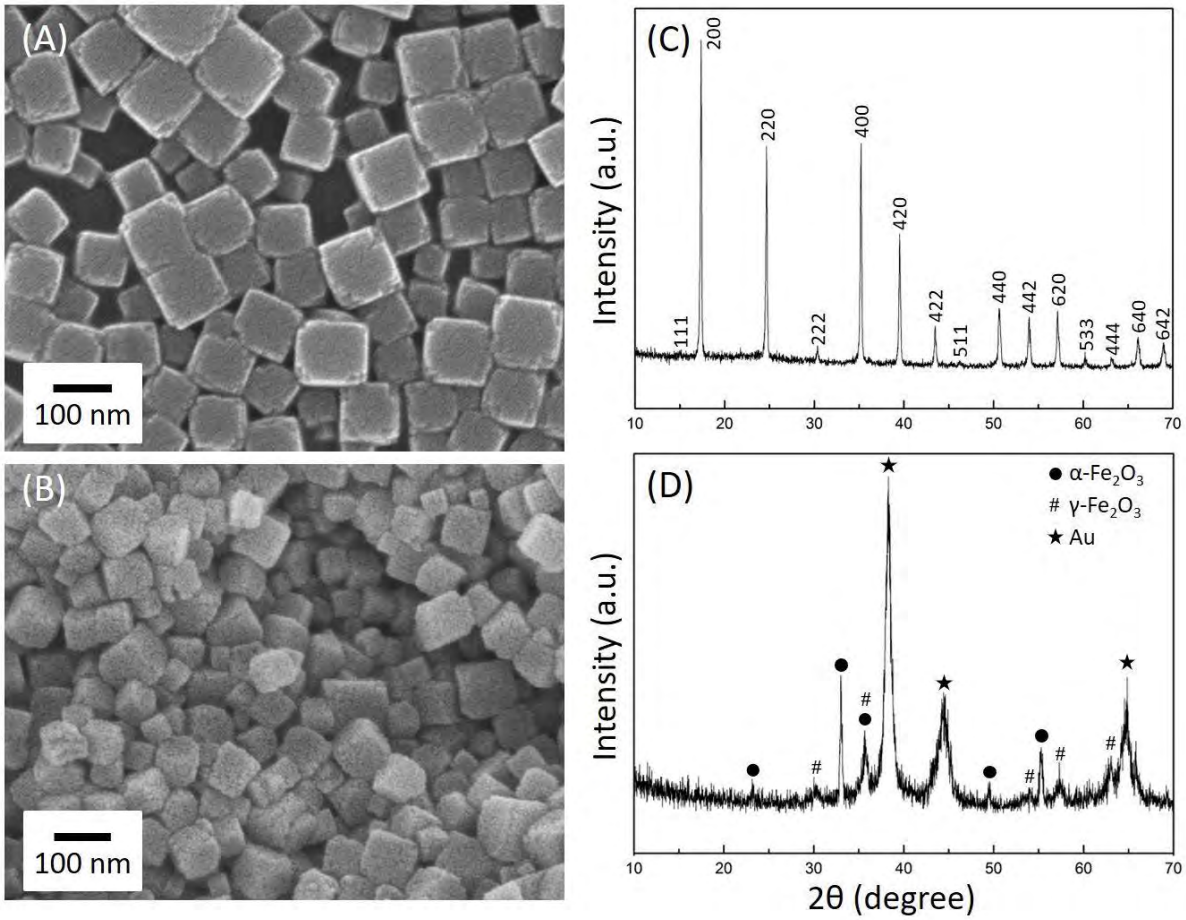

Fig S1. (A-B) SEM images of (A) PB nanocubes and (B) the calcined PB nanocubes. (C-D) Wide-angle XRD patterns of (C) PB nanocubes and (D) Au-loaded nanoporous iron oxide nanocubes.

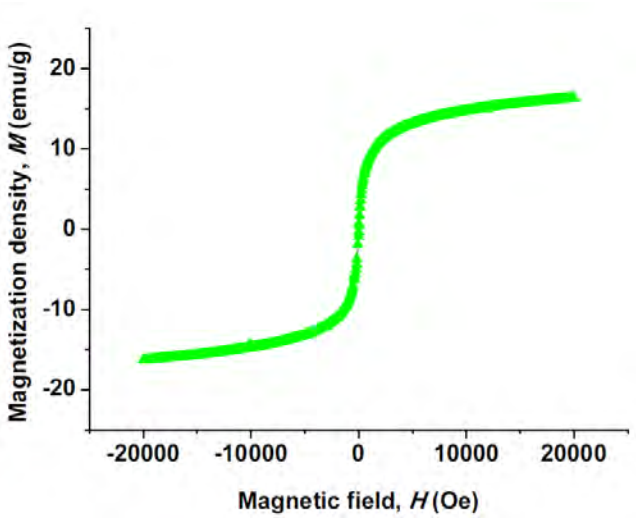

Fig. S2. Magnetization curve measured at 300 K for Au@NPFe_2O_3NC.

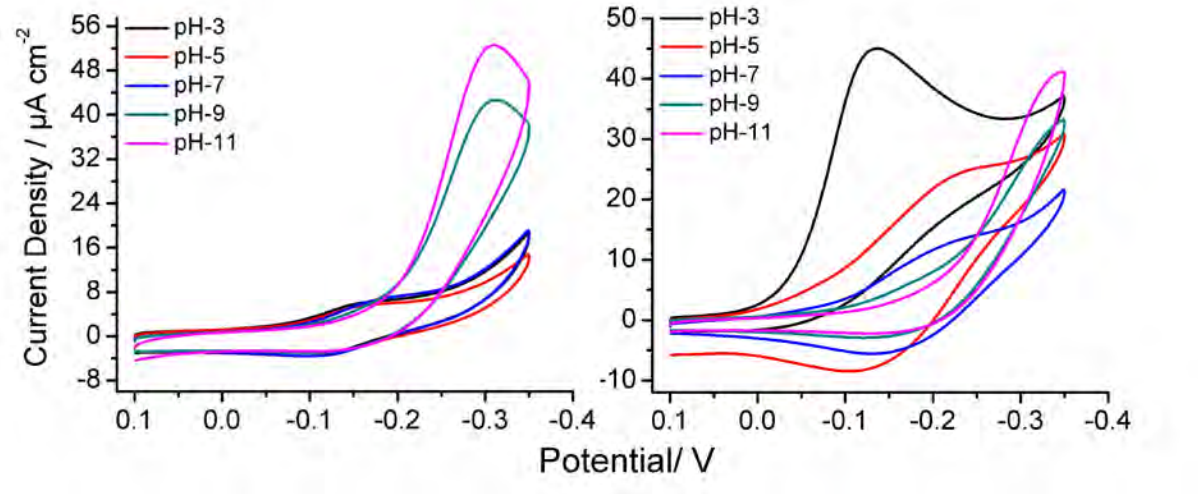

Fig. S3. Cyclic voltammograms at GCE/Bare (left) and GCE/Au@NPFe_2O_3NC (right) at designated pH from 3 to 11 in the presence of 50µM RuHex (0.01M PBS, pH-7, scan rate 50mVs^{-1}).

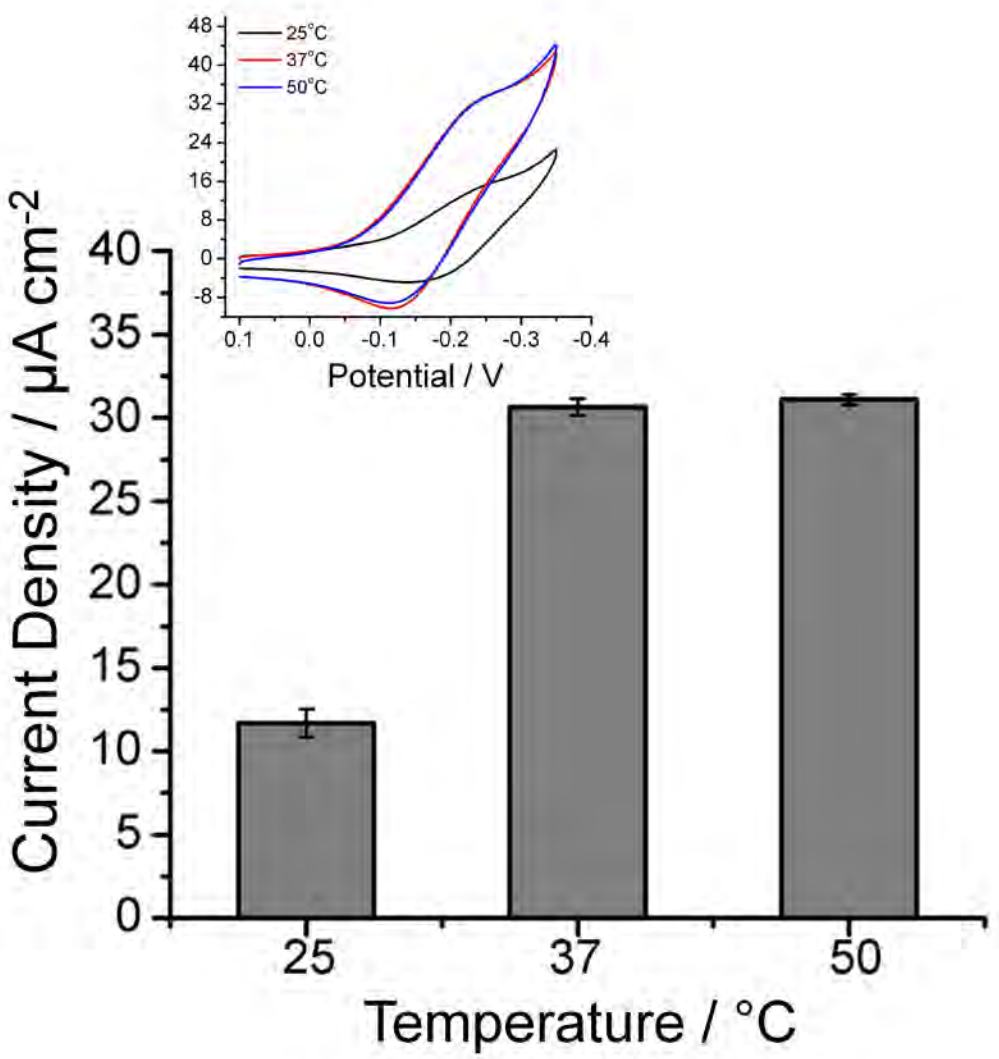

Fig. S4. Cathodic peak currents of GCE/Au@NPFe$_2$O$_3$NC at 25ºC, 37ºC and 50ºC in the presence of 50μM RuHex (0.01M PBS, pH-7, scan rate = 50mVs^{-1}). Inset, corresponding cyclic voltammogram.

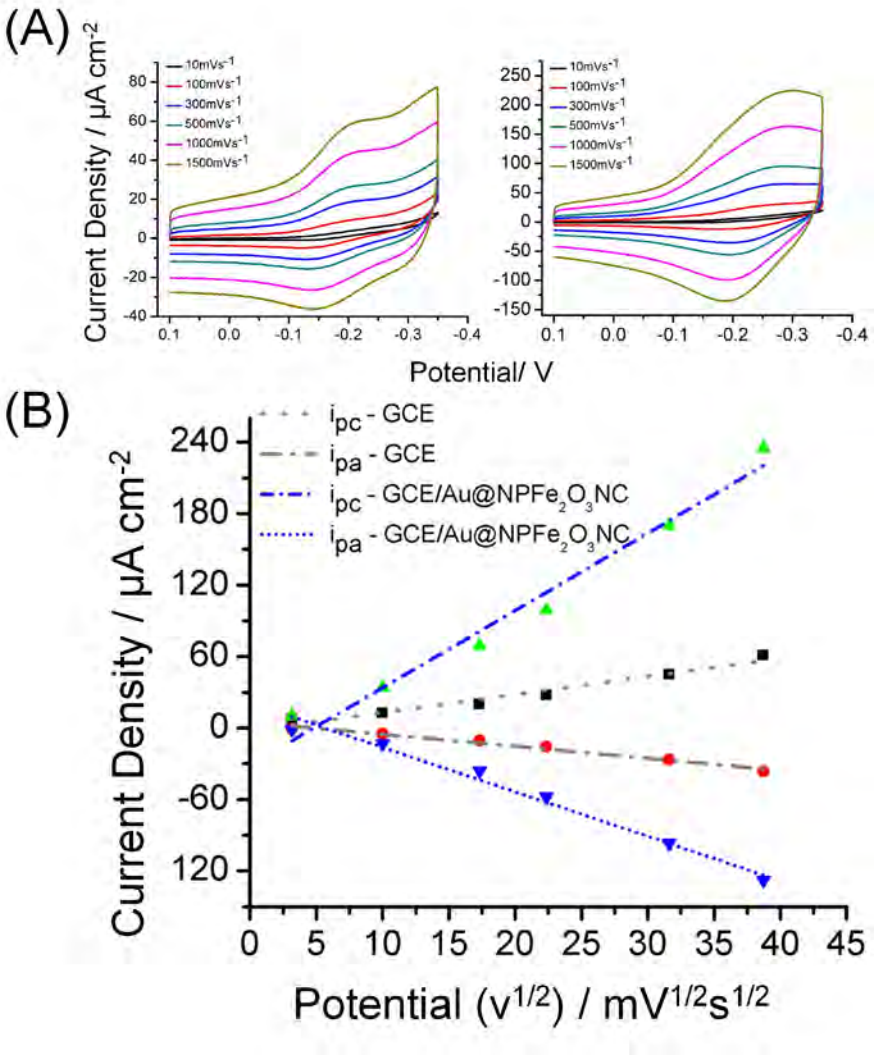

Fig. S5. (A) Cyclic voltammograms obtained at GCE/Bare (top, left) and GCE/Au@NPFe$_2$O$_3$NC (top, right) electrodes at different scan rate (50µM RuHex, 0.01M PBS, pH 7.0). (B) Corresponding curves for i_{pc} and i_{pa} (current density) as a function of $v^{1/2}$.

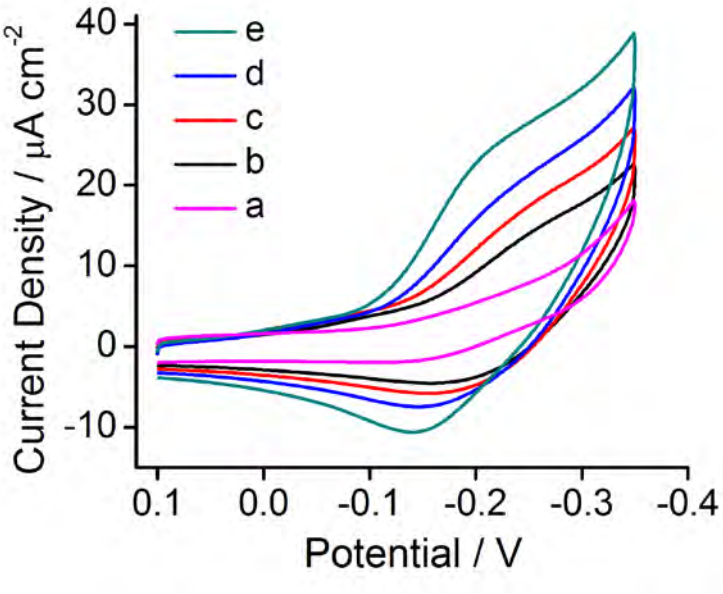

Fig. S6. Cyclic voltammograms of GCE/Au@NPFe$_2$O$_3$NC upon successive addition of RuHex (a-0, b-25, c-50, d-100, and e-200 μM) to the 0.01M PBS (pH-7, scan rate = 50mVs^{-1}).

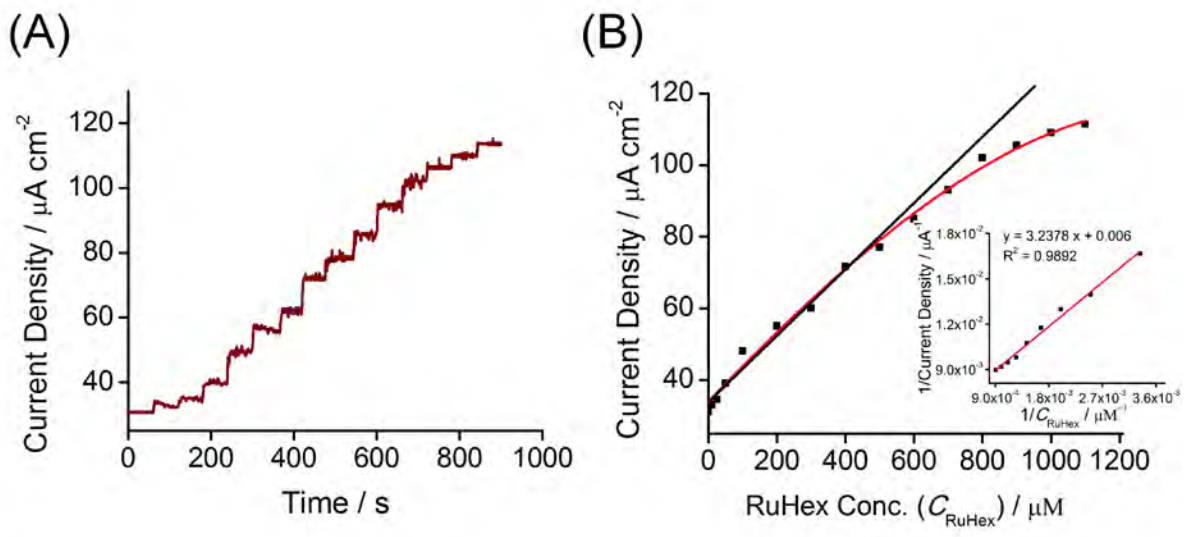

Fig. S7. (A) Amperometric responses of GCE/Au@NPFe_2O_3NC with the successive addition of RuHex solution (10 to 1100μM) into the 0.01M PBS (pH-7); (B) the corresponding calibration plot. Inset of Fig. B: Lineweaver-Burk Model.

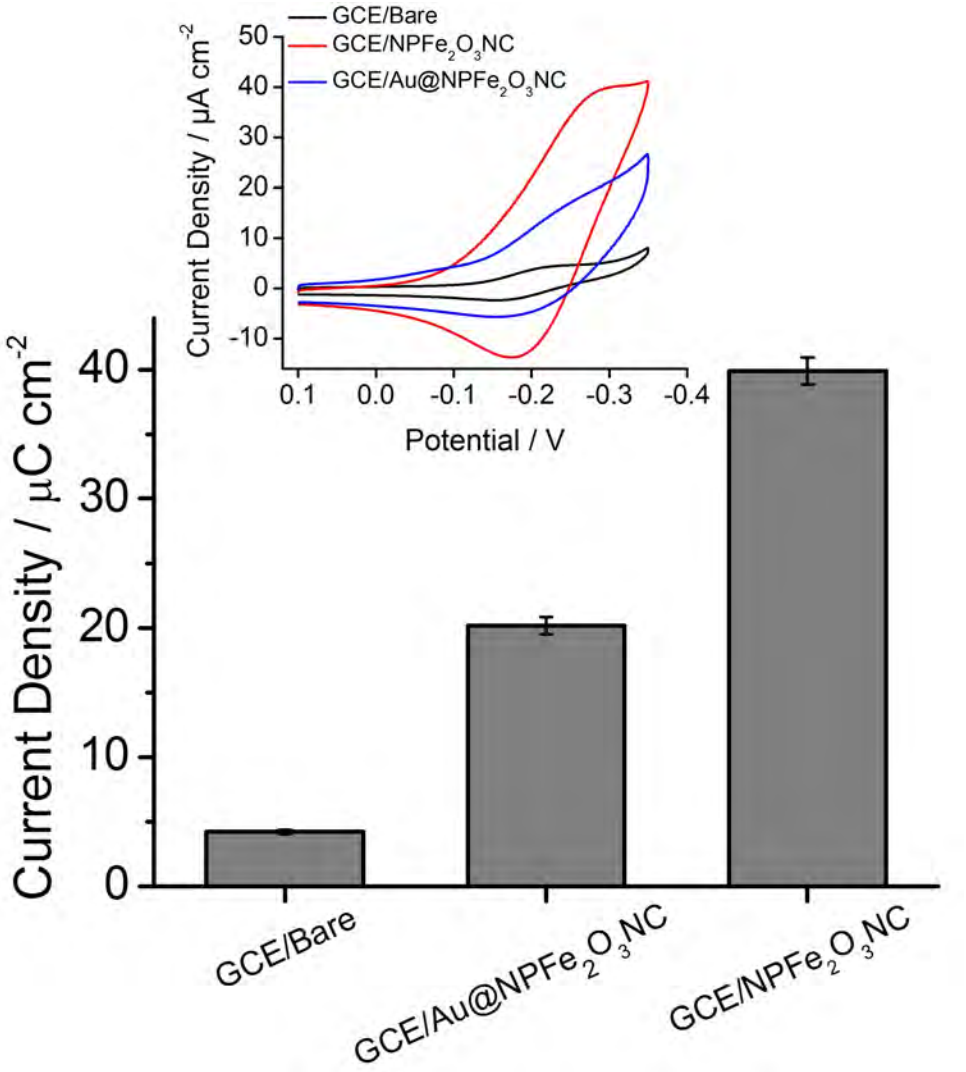

Fig. S8. Cathodic peak currents obtained by bare GCE, Au@$NPFe_2O_3$NC-modified-GCE and $NPFe_2O_3$NC-modified GCE at room temperature, in presence of 50μM RuHex (0.01M PBS, pH-7, scan rate = 50mVs^{-1}). Inset, corresponding cyclic voltammogram.

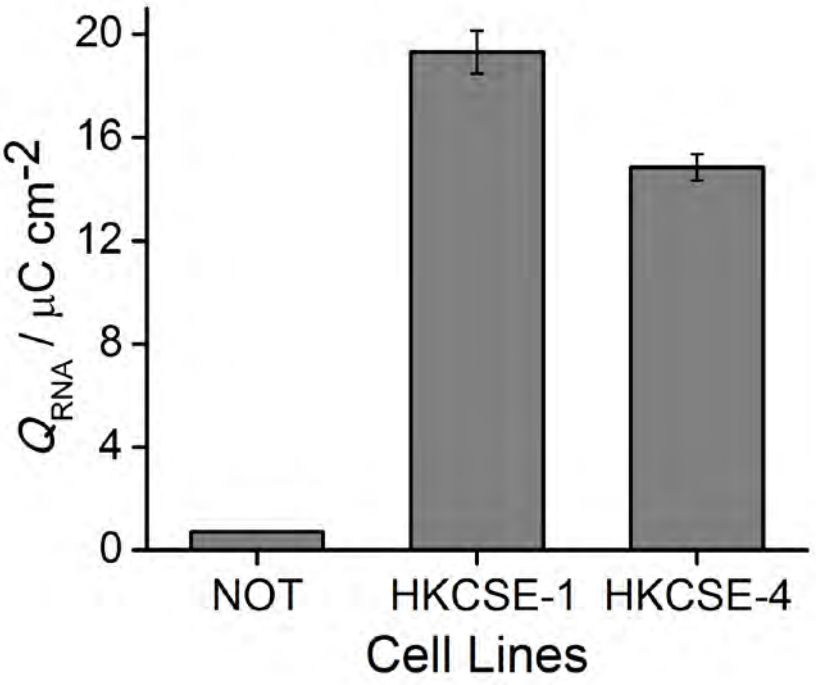

Fig. S9. CC charge generated by the extracted miR-21 from two HKESC-1 and HKESC-4 cell lines.

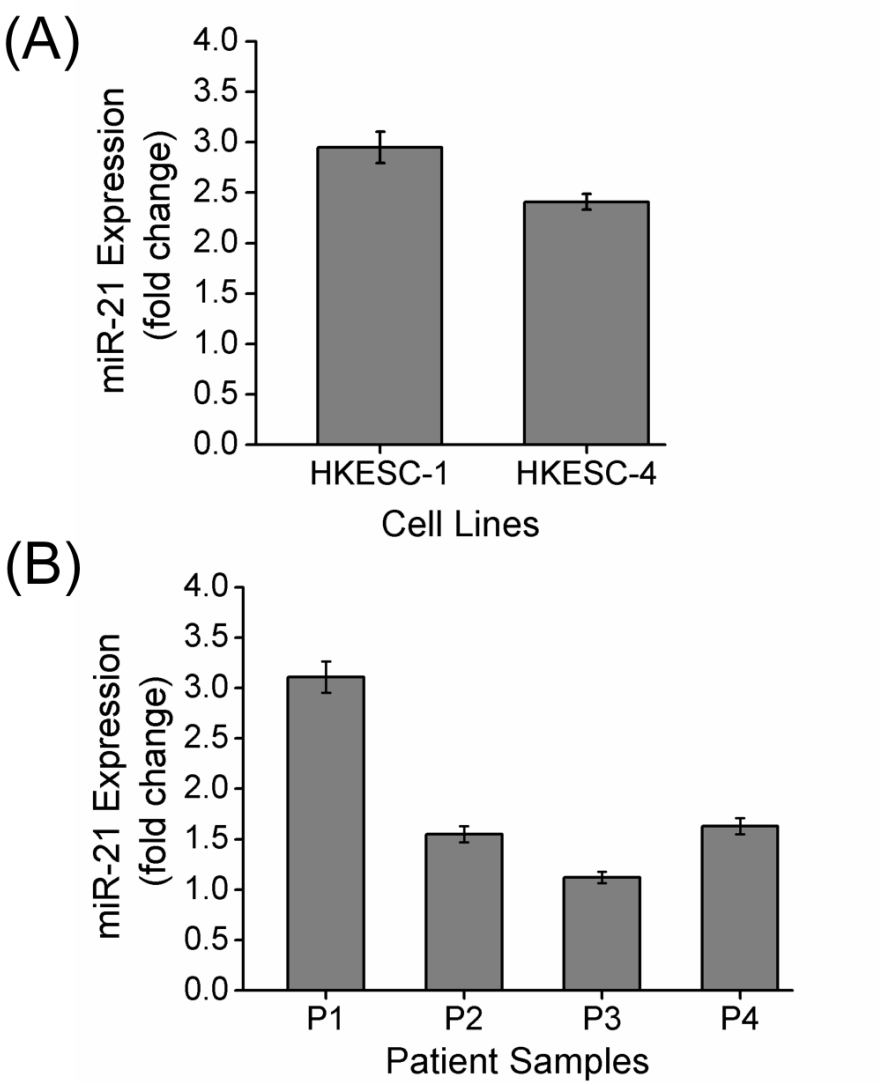

Fig. S10. RT-qPCR validation of miR-21 expression levels in the (A) two ESCC cell lines (B) four tumor tissue samples obtained from the patients with ESCC.

References

1 M. B. Zakaria, A. A. Belik, C. H. Liu, H. Y. Hsieh, Y. T. Liao, V. Malgras, Y. Yamauchi and K. C. Wu, *Chem. Asian J.,* 2015, **10,** 1457.

2 S. Yadav, M. K. Masud, M. N. Islam, V. Gopalan, A. K. Lam, S. Tanaka, *et al.*, *Nanoscale*, 2017. (DOI: 10.1039/C7NR03006A)

3 M. Mustapic, Z. Skoko, Z. Sun, D. R. G. Mitchell, M. S. A. Hossain and S. X. Dou, *Acta Mater.*, 2014, **70**, 298-306.

4 R. D. Zysler, D. Fiorani, A. M. Testa, L. Suber, E. Agostinelli and M. Godinho, *Phys. Rev. B: Condens. Matter. Mater. Phys.*, 2003, **68**, 212408

5 D. Cardillo, M. Tehei, M. S. A. Hossain, M. M. Islam, K. Bogusz, D. Shi, *et al.*, *ACS Appl. Mater. Inter*., 2016, **8**, 5867-5876.

6 L. Lehninger, D. L. Nelson, and M. M. Cox, *Lehninger principles of biochemistry*, W.H.Freeman & Co Ltd, New York, 2005.

7 H. Lineweaver and D. Burk, *J. Am. Chem. Soc.* 1934, **56**, 658-666; A. K. Dutta, S. K. Maji, D. N. Srivastava, A. Mondal, P. Biswas, P. Paul and B. Adhikary, *J. Mol. Catal. A Chem.*, 2012, **360**, 71-77.

8 J. Bard, L. R. Faulkner, *Electrochemical Methods*, John Wiley & Sons, New York, 1980, 199-206.

9 M. J. Shiddiky, A. A. Torriero, C. Zhao, I. Burgar, G. Kennedy, A. M. Bond, *J. Am. Chem. Soc.,* 2009, **131,** 7976-7989.

10 K. M. Koo, A. A. Sina, L. G. Carrascosa, M. J. Shiddiky, and M. Trau, *Anal. Methods,* 2015, **7,** 7042-7054.

11 A. B. Steel, T. M. Herne, and M. J. Tarlov, *Anal. Chem.*, 1998, **70**, 4670-4677.

12 A. Yao, Y. Liu, M. Tabata, H. Zhu, and Y. Miyahara, *Chem. Commun.*, 2014, **50**, 9704-9706.

13 M. H. Haque, V. Gopalan, S. Yadav, M. N. Islam, E. Eftekhari, Q. Li, *et. al.*, *Biosens. Bioelectron.,* 2017, **87**, 615-621.

14 V. Gopalan, S. Pillai, F. Ebrahimi, A. Salajegheh, T. C. Lam, T. K. Le, *et al.*, *Mol. Carcinog.,* 2014, **53**, E36-44.

15 H. Cao, S. Liu, *et al*., *Chem. Commun.*, 2014, **50**, 13315-13318.

16 G. J. Zhang, J. H. Chua, *et al*., *Biosens. Bioelectron.*, 2009, **24**, 2504-2508.

17 M. Bartosik, M. Trefulka, *et al*., *Electrochem. Commun.,* 2013, **33**, 55-58.

18 X. Wu, Y. Chai, R. Yuan, H. Su and J. Han, *Analyst,* 2013, **138**, 1060-1066.

19 F. Bettazzi, E. Hamid-Asl, C. L. Esposito, C. uintavalle, N. Formisano, S. Laschi, *et al.*, *Anal. Bioanal. Chem.*, **405**, 1025-1034.